Negative potentials above the day-side lunar surface in the terrestrial plasma sheet: Evidence of non-monotonic potentials

Andrew Poppe,[1,2,3] Jasper S. Halekas,[3,4] and Mihály Horányi[1,2,3]

Received 8 November 2010; revised 10 December 2010; accepted 21 December 2010; published 28 January 2011.

[1] The Lunar Prospector (LP) Electron Reflectometer (ER) instrument conducted a series of measurements of the lunar surface potential in a variety of conditions. Occasionally, when the Moon was exposed to the terrestrial plasma sheet and in daylight, large, unexpected negative potentials (~−500 V) were measured. In this paper, we compare LP ER measurements with one-dimensional particle-in-cell simulations of the potential above the lunar surface when the Moon is exposed to both solar UV radiation and the terrestrial plasma sheet. The simulations show that large negative potentials will be measured by LP ER due to the presence of stable, non-monotonic potentials. Implications of these measurements to other airless bodies in the solar system are also discussed. **Citation:** Poppe, A., J. S. Halekas, and M. Horányi (2011), Negative potentials above the day-side lunar surface in the terrestrial plasma sheet: Evidence of non-monotonic potentials, *Geophys. Res. Lett.*, *38*, L02103, doi:10.1029/2010GL046119.

1. Introduction

[2] The use of electron reflectometry to measure surface magnetic fields has long been established [*Howe et al.*, 1974; *Anderson et al.*, 1976; *Lin et al.*, 1998], however, the use of this technique to simultaneously probe electrostatic surface potentials is a more recent invention [*Halekas et al.*, 2002]. Electron reflectometry measures surface magnetic fields by exploiting the magnetic mirror effect: electrons with a pitch angle above a critical value, α_o, independent of energy, are reflected from surface magnetic fields, where α_o is dependent on the strength of the spacecraft and surface magnetic fields. Observations of energy-dependent loss cones by the LP ER were interpreted as the result of the combined effects of surface remanent magnetic fields and surface electrostatic potentials [*Halekas et al.*, 2005, 2007, 2008]. The majority of the surface potential measurements confirmed previous models of lunar surface charging, yet some measurements presented challenges to these models. Specifically, the LP ER observed large negative potentials (~−500 V) above the day-side lunar surface while the Moon was exposed to the terrestrial plasma sheet [*Halekas et al.*, 2008]. These measurements contradict the standard point-wise charging calculations [*Manka*, 1973] and *Halekas et al.* [2008] suggested that the presence of non-monotonic potential structures above the lunar surface may account for such large, negative potentials.

[3] Airless bodies throughout the solar system are exposed to both solar ultraviolet (UV) radiation and solar wind and/or magnetospheric plasma. Solar UV radiation stimulates photoemission from the surface of these bodies, and in combination with the collection of ambient plasma, represents the primary surface charging current. These surfaces will charge until the net current to the surface becomes zero; however, the potential structure above the surface can have multiple solutions, namely, a monotonic solution, where the potential constantly increases or decreases, or a non-monotonic solution, where the potential reaches a minimum (or maximum) above the surface, and the gradient of the potential changes sign thereafter. Previous work has addressed the possibility of non-monotonic potentials above airless bodies using both theoretical and simulation methods [*Guernsey and Fu*, 1970; *Fu*, 1971; *Nitter et al.*, 1998; *Poppe and Horányi*, 2010], and found that not only do non-monotonic potential solutions exist, but that they are energetically preferred to the monotonic solution. These potential structures are significant in that they can affect the interpretation of observational results of surface potentials using the electron reflectometry technique. Non-monotonic potentials are likely to be ubiquitous throughout the solar system in various forms, including at Mercury [*Grard*, 1997], asteroids, and various satellites of Mars and the giant planets. These potential structures should be taken into account when modeling or interpreting observations [*Reasoner and Burke*, 1972; *Manka*, 1973; *Dubinin et al.*, 1991; *Roussos et al.*, 2010].

[4] In this paper, we compare a sample LP ER observation of negative potentials above the dayside lunar surface in the terrestrial plasma sheet with a one-dimensional particle-in-cell (PIC) simulation. Section 2 describes the LP ER measurements and Section 3 compares these measurements with the results of the PIC simulation. Section 4 summarizes the results and addresses the impact of these measurements to other bodies in the solar system.

2. Measurements

2.1. Data

[5] This study utilizes data from the Lunar Prospector Electron Reflectometer to characterize electrons of both magnetospheric and lunar origin. The ER employed a top-

[1]Laboratory for Atmospheric and Space Physics, Department of Physics, University of Colorado at Boulder, Boulder, Colorado, USA.
[2]Colorado Center for Lunar Dust and Atmospheric Studies, University of Colorado at Boulder, Boulder, Colorado, USA.
[3]NASA Lunar Science Institute, NASA Ames Research Center, Moffett Field, California, USA.
[4]Space Sciences Laboratory, University of California, Berkeley, California, USA.

0094-8276/11/2010GL046119

hat electrostatic analyzer design to measure the full 3-D electron distribution function. At the time of this study, the energy range of the instrument covered 38 eV to 17 keV. The ER had an intrinsic energy resolution of $\Delta E/E \approx 0.25$, but the onboard processor summed adjacent energy bins together, resulting in an effective $\Delta E/E \approx 0.5$. The ER utilized a 360-degree planar field of view oriented perpendicular to the spin plane to cover all look directions every half-spin (2.5 s), with an angular resolution of 22.5°. Though the ER only had sufficient telemetry to send back full 3-D measurements with an 80 s cadence (corresponding to 120 km separation), the integration lasted only 2.5 s, ensuring an intrinsic spatial resolution for each individual measurement of a few km.

[6] The orbit analyzed in this paper (≈90 min in length) came early in the LP extended mission, at ≈30 km altitude, during a time period when the Moon passed through the center of the terrestrial magnetosphere and encountered the plasma sheet.

2.2. Analysis

[7] We concentrate on data taken in the terrestrial plasma sheet (characterized by increased electron temperatures and decreased magnetic field strength relative to the lobes), when the spacecraft was in an orbit that covered a wide range of solar zenith angles and the surface magnetic field was relatively small (<10 s of nT). Figure 1 shows the magnetic field, the calculated plasma sheet electron temperature, the differential electron energy distribution for five pitch angle bins, the sunlight and magnetic connection flags, and the solar zenith angle of the magnetic footprint. During this time period, we observe an upward-going beam of electrons whenever the spacecraft was on a field line that intersected the Moon, as determined by a straight-line extrapolation of the magnetic field measured at the spacecraft. Previously, such measurements have been used to infer the presence of a negative surface potential below the spacecraft [*Halekas et al.*, 2005, 2008], as expected in shadow or at high solar zenith angle (SZA) in sunlight. However, in this case, we see the upward-going beam of electrons throughout the time period, including times when the magnetic foot point of the field line passing through the spacecraft reached solar zenith angles of up to ≈30°. At these low SZA, the expected photoelectron current from the surface should exceed the magnetospheric electron current by orders of magnitude. This should necessarily force the lunar surface to float to a positive potential, under the assumption that the electrostatic potential varies monotonically above the surface [*Manka*, 1973].

[8] We choose a sample time to investigate in more detail, near the smallest SZA reached on this orbit. We correct the ER data for variations in anode sensitivity, and also apply corrections to the data for the effects of scattered photons and photoelectrons produced on internal surfaces of the instrument by these photons. Due to its large geometric factor, the LP ER was particularly sensitive to these background sources. In order to find the correction, we utilized a spectrum measured at a nearby time (23:09), when the spacecraft was not magnetically connected to the surface. At this time, the measured distribution, other than the photon background, was very well-fit by an isotropic Maxwellian distribution. We therefore subtracted a best-fit Maxwellian to determine the contribution from photon contamination, which should be relatively constant over short time periods. We then subtracted this contamination spectrum from our spectrum of interest to obtain a clean pitch angle-energy spectrum, shown in Figure 2. Analysis of the spectrum yielded an electron temperature of $T_{ps} \approx 350$ eV and an electron density of $n_{ps} \approx 10^5$ m^{-3} [*Halekas et al.*, 2009b]. The corrected flux for down-going pitch angles ($90 < \alpha < 180°$) now shows a nearly isotropic signal, as expected. The electron beam is clearly seen as an enhancement centered around 300 eV for pitch angles, $\alpha < 45°$. While some contamination may remain in the up-going pitch angles at large energies, it remains at a low level compared to the signal of interest. Indeed, none of the corrections described here change the key features of this distribution markedly. At times when the magnetic field aligns with the Earth-Sun line, photon corrections can make a significant difference, especially at small pitch angles; however, at this time the disturbed plasma sheet magnetic field points sixty degrees away from the Sun, therefore, photon corrections have little impact on field-aligned features.

3. Simulations

[9] We used a one-dimensional, particle-in-cell simulation designed to model the electrostatic plasma environment above the day-lit lunar surface while the Moon was in the terrestrial plasma sheet (see *Poppe and Horányi* [2010] for an in-depth description of the PIC code). The simulation models this environment via closed boundary conditions, where one end of the simulation acts as the lunar surface by emitting particles to simulate photoelectrons and absorbing all plasma species, while the opposite end injects the terrestrial plasma sheet. Given the scales required for the simulations (<10 km), a one-dimensional code is adequate for investigating the LP measurements. We used experimentally measured values for the lunar photoelectron current and energy distribution ($J_{ph} = 4.5 \times 10^{-6}$ A/m^2, $T_{ph} = 2.2$ eV [*Feuerbacher et al.*, 1972]) and values representative of the LP ER plasma sheet measurement of Figure 1 ($T_{ps} = 100$–500 eV, $n_{ps} = 10^5$ m^{-3}). Due to the lack of ion observations, all ion parameters are assumed equal to the electron parameters. Previous work has shown that the plasma sheet ion temperature can range up to approximately ten times the electron temperature at lunar distances [*Slavin et al.*, 1985], and preliminary modeling has shown that this may have a small effect on the potential structure. Future work will investigate the role of the ion temperature, as well as various distributions (i.e. kappa distributions) on the potential structure.

[10] Figure 3 shows the potential as a function of height above the lunar surface for various cases of the electron/ion temperature in the plasma sheet, T_{ps}, with the potential normalized to zero at infinity. The potential profiles are consistently non-monotonic, with the region below ~50 m dominated by photoelectrons from the surface and the region above ~50 m dominated by the plasma sheet. The vast majority of the photoelectrons is trapped near the surface, with only the most energetic photoelectrons able to escape out of the near-surface potential well. These photoelectrons are subsequently accelerated by a potential drop of several hundred volts up to the spacecraft position. Additionally, the lower-energy bulk of the plasma sheet electrons

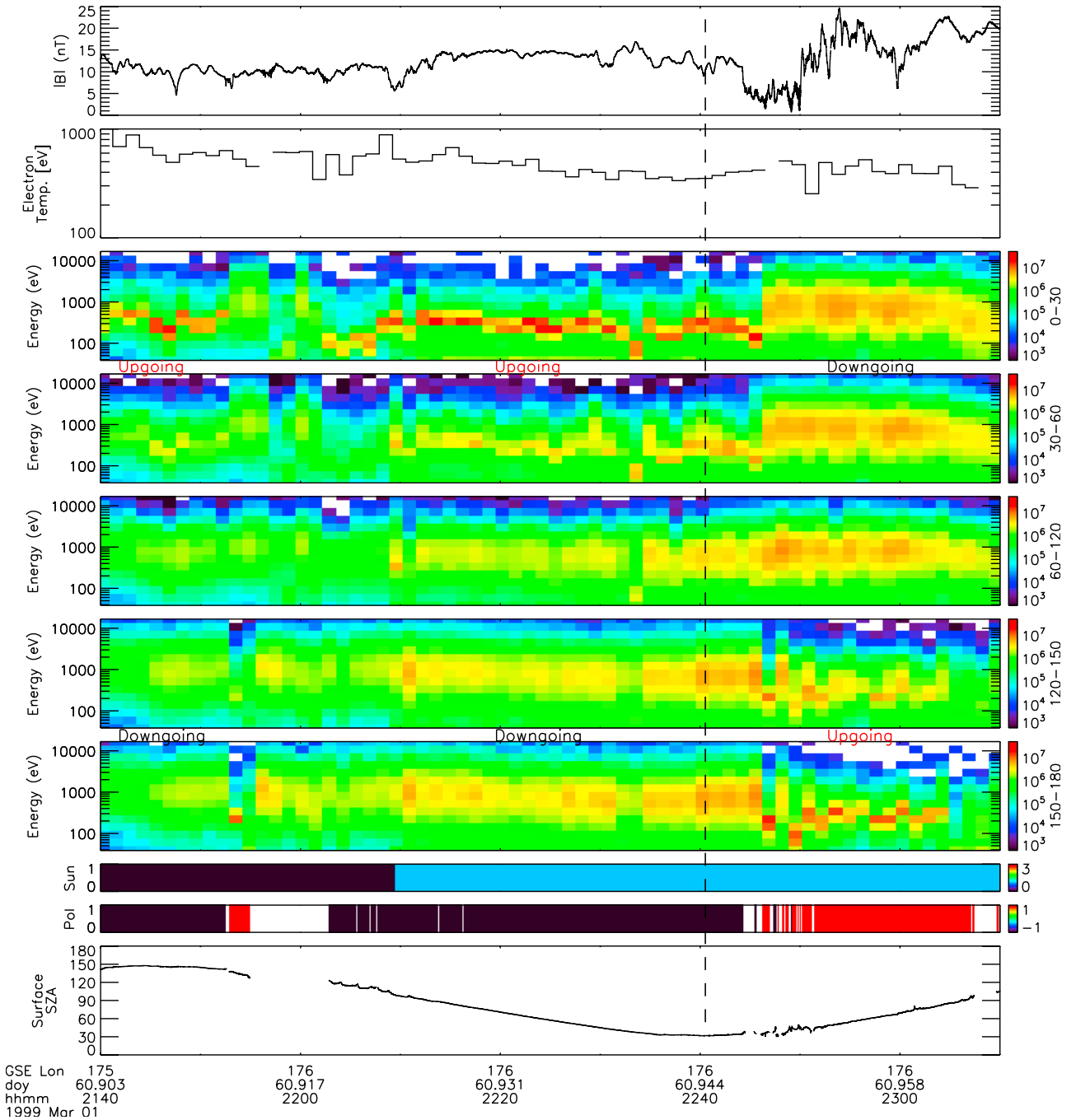

Figure 1. Lunar Prospector orbit (≈90 min) in the terrestrial magnetotail during a series of plasma sheet passages on March 1, 1999, showing the total magnetic field at the spacecraft, the derived plasma sheet electron temperature, electron differential energy flux [eV/(cm^2 sr s eV)] in five different pitch angle channels (0–30°, 30–60°, 60–120°, 120–150°, 150–180°), sun/shadow color bar "Sun" (blue = sun, black = shadow), magnetic connection to surface "Pol" (assuming no field curvature, red = positive connection, black = negative connection, white = no connection), and solar zenith angle (SZA) of connection to surface. Lunar Prospector observes an upward-going electron beam during this time period whenever magnetically connected to the surface, in both sunlight and shadow.

are reflected by the potential barrier and return to the spacecraft.

[11] In order to provide the best comparison to the 1-d model results, we calculated the reduced distribution function, $f(v_{||})$, and computed the ratio of upward going to downward going phase space density as a function of parallel energy, for the case discussed in Section 2. To accomplish this, we first re-gridded the measured distribution in terms of parallel and perpendicular velocity, and then calculated, $f(v_{||}) = \int f(v_{||}, v_\perp) 2\pi v_\perp dv_\perp$. In order to reduce the confounding effects of magnetic mirroring, which cannot be captured in a 1-d simulation, we included only data within 45° of 0° and 180° pitch angle in the integral. This selection eliminates electrons that mirror magnetically

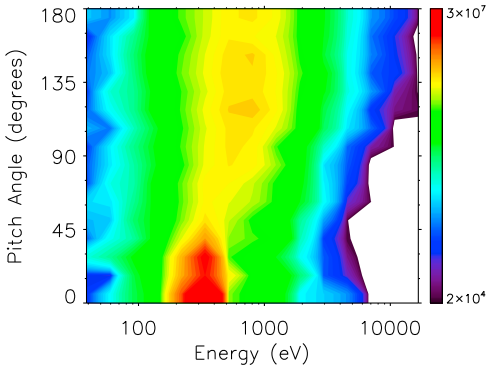

Figure 2. Energy pitch angle spectrogram at 22:40:10 on March 1, 1999, shown in units of electron differential energy flux [eV/(cm^2 sr s eV)]. Counts from scattered photons and internally produced photoelectrons have been approximately subtracted, as described in the text. Some residual background counts may remain at energies above 1000 eV in the upward-going pitch angles. The upward-going beam is seen at energies of ~200–500 eV and pitch angles of 0–45°.

before reaching the near-surface sheath region. Though the magnetic mirror force still plays some role in the dynamics of the remaining electrons, the selected population provides the most direct comparison to the simulation.

[12] Figure 4 compares the modeled differential energy distributions for both plasma sheet electrons and photoelectrons with the LP ER measurements, all normalized to the downward plasma sheet electron differential energy distribution. Both the model and the LP measurements show a ratio of approximately unity for energies, $E < 150$ eV, and a peak in the upward/downward ratio at energies, $E \approx 220$ eV. The disagreement in the spread of the 220 eV peak is due to the intrinsic LP energy resolution, which acts to smear out the electron flux in energy. As the model shows, the lower energy portion is composed of the reflected plasma sheet

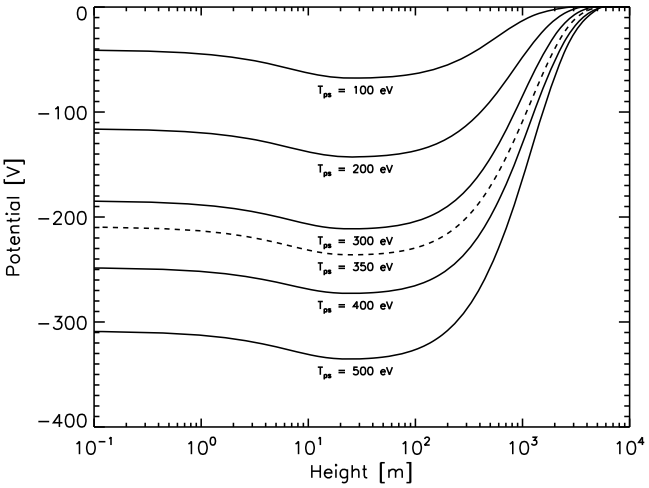

Figure 3. The potential as a function of height above the lunar surface from the simulations for five different cases (solid lines) of the plasma sheet electron temperature, T_{ps}. Additionally, the potential for the T_{ps} = 350 eV case is also shown.

electrons, while the peak is composed of escaping photoelectrons accelerated to energies matching the potential barrier above the lunar surface. While the energy resolution of the LP ER smears out the photoelectron peak to some degree, the agreement between the data and the PIC model confirms that the apparent negative surface charging is in fact due to large, non-monotonic potential structures above the lunar surface.

4. Summary and Discussion

[13] We have presented measurements indicating large negative surface potentials on the dayside lunar surface while in the terrestrial plasma sheet that contradict the standard point-wise charging theory for the lunar surface [*Manka*, 1973]. A one-dimensional particle-in-cell simulation of this environment revealed that the LP ER measurements are best explained by the presence of stable, non-monotonic potentials above the lunar surface. Additionally, preliminary work suggests that non-monotonic potentials may also be present while the Moon is in the solar wind (J. S. Halekas et al., manuscript in preparation, 2010), and on the lunar nightside. Non-monotonic potentials on the lunar nightside could explain a deficiency in observed lunar secondary electrons, as the potential would serve to trap the secondaries near the surface [*Halekas et al.*, 2009a]. The model also predicts that while electron reflectometry measurements will sense a negative potential, the lunar surface will be charged positively due to the change in slope of the potential. By keeping track of particles emitted and absorbed at the left boundary [see *Poppe and Horányi*, 2010], the model indicates that the lunar surface charge density is approximately +3.9 × 10^{-11} C/m^2, regardless of the plasma sheet parameters. The independence of the surface charge density from the external plasma parameters is due to the

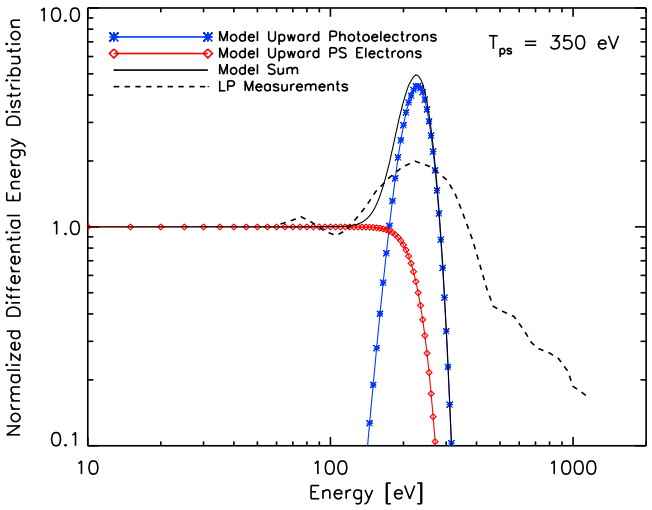

Figure 4. The differential energy distribution of escaping photoelectrons (blue curve), reflected (upward-traveling) plasma sheet electrons (red curve), the sum of photo- and reflected plasma sheet electrons (black curve), and LP ER measurements (dashed line), all normalized by the downward-traveling plasma sheet electron differential energy distribution, from the simulation with T_{ps} = 350 eV. LP-measured fluxes greater than 500 eV are most likely due to remaining noise contamination.

shielding effect of the non-monotonic potential, and such potentials should be taken into account when estimating surface charge densities.

[14] The measurement of non-monotonic potentials above the Moon suggests that this process may be present at all airless bodies throughout the solar system, including at Mercury [*Grard*, 1997], the Martian moons [*Dubinin et al.*, 1991], and the satellites of the giant planets [*Roussos et al.*, 2010]. Measurements around these bodies should be investigated for any evidence of non-monotonic potentials. Non-monotonic potentials above airless surfaces will also impact the study of electrostatic charging and transport of dust grains and should be taken into account in any models thereof [*Ip*, 1986; *Colwell et al.*, 2005; *Stubbs et al.*, 2006; *Colwell et al.*, 2009; *Poppe and Horányi*, 2010]. Spacecraft may also generate non-monotonic potentials when photoemitting and such an effect should be considered in spacecraft design and data interpretation [*Ergun et al.*, 2010]. Future work will continue to investigate the presence of these non-monotonic potential structures, including any possible dependence on the strength of surface remanent magnetic fields, and the role of instabilities and waves due to the interaction between the upward accelerated beam of photoelectrons and the solar wind flow towards the Moon.

[15] **Acknowledgments.** The authors thank G. T. Delory for helpful conversations on this subject. A. P. was supported by the NASA Earth and Space Science Fellowship program, grant NNX08BA17H. M. H. was supported by the Colorado Center for Lunar Dust and Atmospheric Studies of NASA's Lunar Science Institute and by NASA's LASER program, grant NNX08AY77G. J. S. H. was supported by the NASA Lunar Science Institute.

References

Anderson, K. A., et al. (1976), Measurements of lunar and planetary magnetic fields by reflection of low energy electrons, *Space Sci. Instrum.*, *1*, 439–470.

Colwell, J. E., et al. (2005), Dust transport in photoelectron layers and the formation of dust ponds on Eros, *Icarus*, *175*, 159–169.

Colwell, J. E., et al. (2009), Lunar dust levitation, *J. Aero. Eng.*, *22*, 2–9.

Dubinin, E. M., et al. (1991), Plasma and magnetic field effects associated with Phobos and Deimos tori, *Planet. Space Sci.*, *39*(1–2), 113–121.

Ergun, R. E., et al. (2010), Spacecraft charging and ion wake formation in the near-Sun environment, *Phys. Plasmas*, *17*, 072903.

Feuerbacher, B., et al. (1972), Photoemission from lunar surface fines and the lunar photoelectron sheath, *Proc. Lunar Sci. Conf.*, *2*, 2655–2663.

Fu, J. H. M. (1971), Surface potential of a photoemitting plate, *J. Geophys. Res.*, *76*(10), 2506–2509.

Grard, R. (1997), Photoemission on the surface of Mercury and related electrical phenomena, *Planet. Space Sci.*, *45*(1), 67–72.

Guernsey, R. L., and J. H. M. Fu (1970), Potential distribution surrounding a photo-emitting plate in a dilute plasma, *J. Geophys. Res.*, *75*(16), 3193–3199.

Halekas, J. S., D. L. Mitchell, R. P. Lin, L. L. Hood, M. H. Acuña, and A. B. Binder (2002), Evidence for negative charging of the lunar surface in shadow, *Geophys. Res. Lett.*, *29*(10), 1435, doi:10.1029/2001GL014428.

Halekas, J. S., R. P. Lin, and D. L. Mitchell (2005), Large negative lunar surface potentials in sunlight and shadow, *Geophys. Res. Lett.*, *32*, L09102, doi:10.1029/2005GL022627.

Halekas, J. S., G. T. Delory, D. A. Brain, R. P. Lin, M. O. Fillingim, C. O. Lee, R. A. Mewaldt, T. J. Stubbs, W. M. Farrell, and M. K. Hudson (2007), Extreme lunar surface charging during solar energetic particle events, *Geophys. Res. Lett.*, *34*, L02111, doi:10.1029/2006GL028517.

Halekas, J. S., G. T. Delory, R. P. Lin, T. J. Stubbs, and W. M. Farrell (2008), Lunar Prospector observations of the electrostatic potential of the lunar surface and its response to incident currents, *J. Geophys. Res.*, *113*, A09102, doi:10.1029/2008JA013194.

Halekas, J. S., et al. (2009a), Lunar Prospector measurements of secondary electron emission from lunar regolith, *Planet. Space Sci.*, *57*, 78–82.

Halekas, J. S., G. T. Delory, R. P. Lin, T. J. Stubbs, and W. M. Farrell (2009b), Lunar surface charging during solar energetic particle events: Measurement and prediction, *J. Geophys. Res.*, *114*, A05110, doi:10.1029/2009JA014113.

Howe, H. C., R. P. Lin, R. E. McGuire, and K. A. Anderson (1974), Energetic electron scattering from the lunar remanent magnetic field, *Geophys. Res. Lett.*, *1*(3), 101–104.

Ip, W.-H. (1986), Electrostatic charging and dust transport at Mercury's surface, *Geophys. Res. Lett.*, *13*(11), 1133–1136.

Lin, R. P., et al. (1998), Lunar surface magnetic fields and their interaction with the solar wind: Results from Lunar Prospector, *Science*, *281*, 1480–1484.

Manka, R. H. (1973), Plasma and potential at the lunar surface, in *Photon and Particle Interactions With Surfaces in Space*, *Astrophys. Space Sci.*, vol. 37, edited by R. J. L. Grard, pp. 347–361, Reidel, Dordrecht, Neth.

Nitter, T., O. Havnes, and F. Melandsø (1998), Levitation and dynamics of charged dust in the photoelectron sheath above surfaces in space, *J. Geophys. Res.*, *103*(A4), 6605–6620.

Poppe, A., and M. Horányi (2010), Simulations of the photoelectron sheath and dust levitation on the lunar surface, *J. Geophys. Res.*, *115*, A08106, doi:10.1029/2010JA015286.

Reasoner, D. L., and W. J. Burke (1972), Characteristics of the lunar photoelectron layer in the geomagnetic tail, *J. Geophys. Res.*, *77*(34), 6671–6687.

Roussos, E., N. Krupp, H. Krüger, and G. H. Jones (2010), Surface charging of Saturn's plasma-absorbing moons, *J. Geophys. Res.*, *115*, A08225, doi:10.1029/2010JA015525.

Slavin, J. A., E. Smith, D. Sibeck, D. Baker, R. Zwickl, and S.-I. Akasofu (1985), An ISEE 3 study of average and substorm conditions in the distant magnetotail, *J. Geophys. Res.*, *90*(A11), 10,875–10,895.

Stubbs, T. J., et al. (2006), A dynamic fountain model for lunar dust, *Adv. Space Res.*, *37*, 59–66.

J. S. Halekas, Space Sciences Laboratory, University of California, 7 Gauss Way, Berkeley, CA 94720, USA. (jazzman@ssl.berkeley.edu)

M. Horányi and A. Poppe, Laboratory for Atmospheric and Space Physics, Department of Physics, University of Colorado at Boulder, UCB 392, Boulder, CO 80309, USA. (horanyi@colorado.edu; poppe@lasp.colorado.edu)